



ELSEVIER

## Laser-damage of cleaved and polished $\text{CaF}_2$ at 248 nm

S. Gogoll<sup>a</sup>, E. Stenzel<sup>a</sup>, H. Johansen<sup>b</sup>, M. Reichling<sup>a,\*</sup>, E. Matthias<sup>a</sup>

<sup>a</sup> *Fachbereich Physik, Freie Universität Berlin, Arnimallee 14, 14195 Berlin, Germany*

<sup>b</sup> *Max-Planck-Institut für Mikrostrukturphysik, Weinberg 2, 06120 Halle (Saale), Germany*

### Abstract

We investigated the surface damage of  $\text{CaF}_2$  induced by irradiation with 248 nm/14 ns laser pulses. Experiments were carried out in single shot mode in air. The photoacoustic deflection technique was utilized for in situ damage detection and irradiated spots were inspected by scanning electron microscopy. Fracture along the natural cleavage planes was observed. Comparison of cleaved and polished samples in connection with modelling the thermoelastic response of the crystal during damage reveals that polishing causes enhanced surface absorption. Damage topography at the periphery of the irradiated spots was used to obtain a rough estimate of the temperature rise leading to fracture. Electron microscopy shows surface modifications of weakly irradiated spots where no ablation or cracking could be detected.

### 1. Introduction

Laser damage of transparent materials has been the subject of investigation for many years (e.g. Refs. [1–3]). Such studies are of interest for a better understanding of the fundamental damage processes. The damage resistivity of wide bandgap crystals is also of great practical importance for high power UV laser optics. The first question of laser interaction with transparent materials is the mechanism of energy deposition for which, in commercially available crystals, impurities and lattice defects of various origins are responsible. Especially the polishing procedure may cause severe surface contamination and evoke structural defects. For standard mechanical polishing, a surface layer with a disturbed crystalline structure of about 0.3  $\mu\text{m}$  thickness was observed [4,5]. These mechanically introduced dislocations can lead to additional electronic states in the bandgap, which strongly enhance the absorption of laser energy.

To elucidate the damage mechanism much work has been done using mass- and energy-selecting techniques like time-of-flight and quadrupole mass spectroscopy [3,6,7]. An appropriate tool to investigate damage morphology is scanning electron microscopy (SEM) [8–10]. In the present paper a careful topographical analysis of the damage structure is presented using backscattered and secondary electron techniques. Two main damage features are observed: fracture crossing the sample surface and cracking at a certain depth parallel to the surface. Such cracking often results in tiles loosely bound to the surface

or completely removed. We suggest a thermoelastic model that explains the fracture crossing the surface. It also enables us to estimate absorption and temperature rise at the surface. As described in detail elsewhere [11], the cracking parallel to the surface can be explained by enhanced surface absorption decreasing exponentially with depth. In order to verify this we compare in this contribution polished and cleaved surfaces combining the probe beam deflection (PBD) technique [12] with subsequent SEM investigations. Electron microscopy was carried out on uncoated surfaces to enable a sensitive detection of surface modifications.

### 2. Experimental setup

The damage behaviour was measured under normal conditions in an 1-on-1 irradiation mode. An excimer laser supplied a good top hat profile with 14 ns pulses of 248 nm wavelength. The beam was focused on the front side of the crystal into an oval-shaped spot with principal axes of 100 and 170  $\mu\text{m}$ . Pulse energy was varied in the range of 0.3 to 40  $\text{J}/\text{cm}^2$ . The laser light was focused by a lens of short focal length to avoid rear side damage of the crystal. The acoustic or shock wave emitted into the surrounding air was detected via the deflection of a probe beam guided parallel to the surface [12]. We monitored both, deflection amplitude and arrival time.

The experiments were performed on cleaved and optically polished UV-grade  $\text{CaF}_2(111)$  single crystals, purchased from Karl Korth company, Kiel. To ensure a reliable comparison, polished and cleaved surfaces of the same crystal were used.

\* Corresponding author. Fax +49 30 838 6059, e-mail reichling@matth1.physik.fu-berlin.de

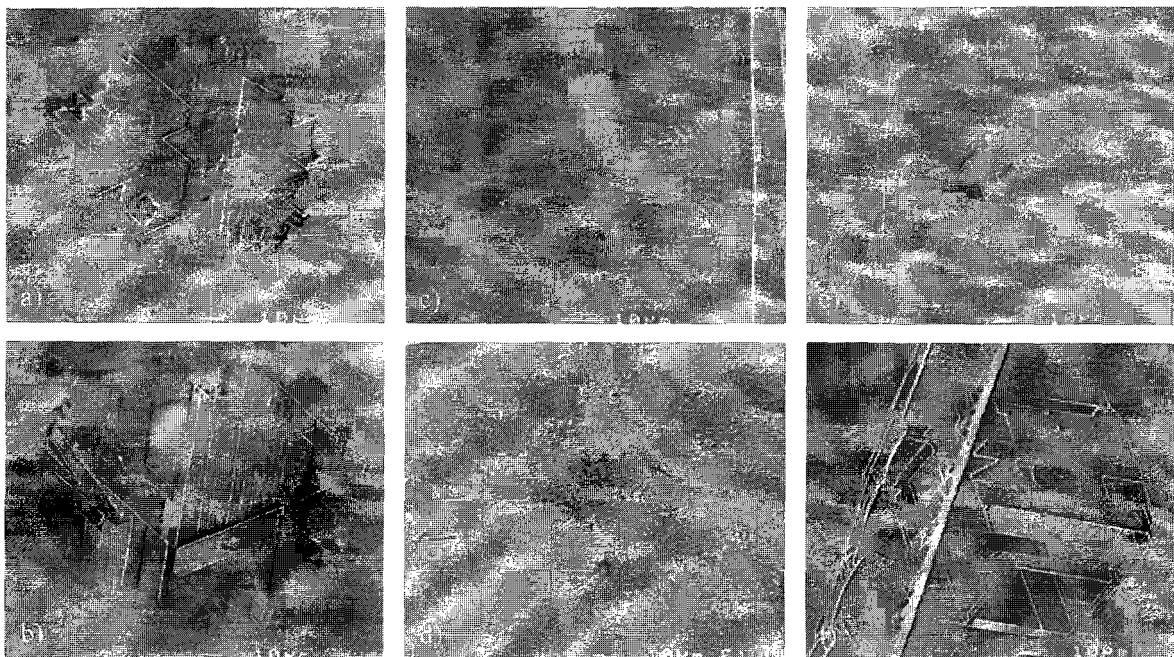


Fig. 1. SEM micrographs in secondary electron mode of different spots on  $\text{CaF}_2(111)$ , each irradiated with a single (248 nm/14 ns) excimer laser pulse: (a) 15 and (b) 28.3  $\text{J}/\text{cm}^2$  on a polished surface, (c) 16 and (d) 32.1  $\text{J}/\text{cm}^2$  on a terrace of a cleaved surface, (e) 16.9 and (f) 31.1  $\text{J}/\text{cm}^2$  at steps of a cleaved surface.

Scanning electron microscopy of the irradiated sample was carried out using a JEOL field emission SEM 6300F. In contrast to usual SEM examinations of insulators, in which samples are conductively coated for the purpose of charge elimination, images were taken of uncoated crystal surfaces [13]. To obtain different contrast features due to sample charging the primary electron energy was varied between 0.7 and 10 keV.

### 3. Results

SEM investigations reveal a greatly different damage onset for polished and cleaved crystals. Nevertheless, once massive damage has occurred, the morphology is nearly the same for both surfaces. In the following we first describe these common features.

Typical damage structures of a polished surface for fluences above the massive damage threshold of 10  $\text{J}/\text{cm}^2$  can be seen in Figs. 1a and 1b where the incident fluence was significantly higher (28.3  $\text{J}/\text{cm}^2$ ). No principally different features due to the variation of laser fluence are visible. Fracture mostly happens along the natural (111)-cleavage planes. Thus, tiles in the shape of equilateral triangles, isosceles trapeziums and parallelograms are formed and often, at higher fluences, removed from the surface. In the center of the spot large tiles with an area of approximately 100  $\mu\text{m}^2$  dominate. Their thicknesses de-

pend on the incident laser fluence and lie in the range of 0.5  $\mu\text{m}$  [11]. At the periphery the density of cracks is remarkably higher and the tile area consequently much smaller. This becomes evident in the magnified image shown in Fig. 2, where a distance of about 1  $\mu\text{m}$  between neighbouring cracks is found.

To explain these fracture features at the spot periphery we developed a model based on simple thermoelastic considerations. This enables us to estimate the temperature rise and the absorption coefficient at the surface. In trans-

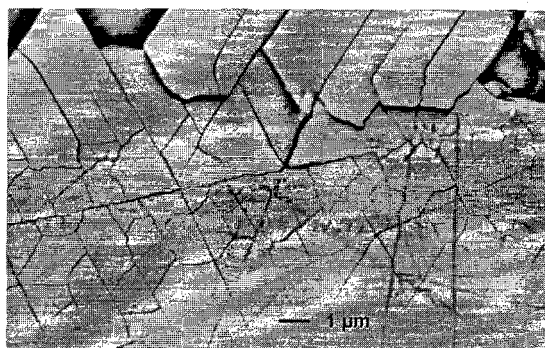


Fig. 2. SEM micrograph in composition contrast of the rim region of a spot irradiated with a single laser pulse of 11.9  $\text{J}/\text{cm}^2$ . This image reveals a high density of cross cracks that can only be found at the spot margin.

parent crystals only a small part of the incident laser energy is absorbed. Since damage is only visible in the near-surface region, we assume that absorption mainly takes place there. Concerning a thermal damage mechanism, a homogeneous lateral heating within the irradiated spot can be assumed, since the mean distance between defects is much smaller than the thermal diffusion length. A typical bulk defect density of roughly  $10^{16}$ – $10^{17}$   $\text{cm}^{-3}$  [14,15] results in an average defect distance of a few tens of nanometers, whereas the thermal diffusion length  $\sqrt{2D\tau}$  in  $\text{CaF}_2$  for a 14 ns laser pulse is 320 nm (with heat diffusivity  $D$  and laser pulse length  $\tau$ ). The resulting temperature increase at the surface causes a thermoelastic displacement. At the spot rim the lateral temperature variation  $T_s(r)$  gives rise to shear stress which causes fracture there. Be  $u_z$  the expansion perpendicular to the surface, the stress is given by ( $G$ : shear modulus)

$$\sigma_{rz} = G\partial u_z / \partial r. \quad (1)$$

Defining the damage depth  $d$ , which is the typical observed tile thickness of about  $1/2$   $\mu\text{m}$  [11], as the depth of the heated layer we can approximate the vertical displacement by [16]

$$u_z = -\beta \int_0^{\infty} T(r, z) dz \approx -\beta \frac{T_s(r)}{2} d, \quad (2)$$

where  $\beta$  is the linear thermal expansivity. This results in

$$\sigma_{rz} = -G\beta \frac{d}{2} \frac{\partial T_s(r)}{\partial r} \quad (3)$$

As the temperature rise at the surface is proportional to the incident laser fluence,  $T_s$  is characterized by the beam profile parameters and the absorbance. For the calculations we assume a circular shape of the laser spot with diameter  $w$  at half maximum and rim width  $f$ , which is roughly 8  $\mu\text{m}$ . Hence  $T_s$  has its maximum value  $T_m$  in the center and decreases over the border area:

$$T_s(r) = T_m, \quad \text{for } 0 < r < \frac{w-f}{2},$$

$$T_s(r) = T_m \frac{w+f-2r}{2f}, \quad \text{for } \frac{w-f}{2} < r < \frac{w+f}{2}, \quad (4)$$

$$T_s(r) = 0, \quad \text{for } r > \frac{w+f}{2}.$$

Fracture stress occurs exclusively at the rim since only gradients in temperature contribute. Hence we obtain:

$$\sigma_{rz} = G\beta \frac{d}{2f} T_m, \quad \text{for } \frac{w-f}{2} < r < \frac{w+f}{2}. \quad (5)$$

Fracture takes place, when this stress exceeds the tensile strength. This leads in the indicated range to the large density of cracks, as observed in Fig. 2. As scratches resulting from the polishing procedure enhance the ten-

dency to fracture [17], a fracture strength of  $10^{-3}$ – $10^{-4}$   $Y$  is commonly used ( $Y$ : Young modulus) [18,19]. When inserting this value into Eq. (5) the threshold temperature rise lies between 400 and 4000°C. To obtain such temperatures an energy deposition of

$$E = \pi \left( \frac{w}{2} \right)^2 d \rho C_v \frac{T_m}{2} \quad (6)$$

is required, where  $\rho$  is the specific density and  $C_v$  the heat capacity. It amounts to 4–40  $\mu\text{J}$ . In connection with the observed threshold fluence of  $10$   $\text{J}/\text{cm}^2$  this corresponds to an absorption of about 0.3–3% of the total laser energy in the surface-near region. This energy absorption is consistent with values obtained by calorimetric measurements on  $\text{CaF}_2$  [20,21]. The assumption of an enhanced absorption near the surface was also confirmed by Gallant et al. [20], who observed a strong dependence on surface preparation.

Like the temperature variation in lateral direction causes a cross cracking, a temperature gradient into the depth can actuate fracture parallel to the (111) surface resulting in the formation of the tiles seen in Figs. 1a and 1b. Both vertical and lateral fracture can be explained by assuming an enhanced surface absorption due to the polishing procedure. A convenient cross-check for this assumption is a comparative measurement on polished and cleaved surfaces. As shown by Gogoll et al. [11] mirage measurements revealed a remarkably higher resistivity against laser irradiation for cleaved crystals. In the present paper the mirage experiments have been combined with an individual SEM observation of each irradiated spot in order to clarify where damage preferentially takes place. Fig. 1 displays a set of typical SEM images. Polished surfaces (Figs. 1a and 1b) show the earliest onset of massive damage, which takes place almost uniformly over the entire irradiated area. Thus the assumption of an enhanced surface absorption for the polished surface is justified. For the cleaved surfaces damage was observed to start at or near steps (Figs. 1e and 1f), whereas terraces can only be destroyed by highest fluences (Figs. 1c and 1d).

In Fig. 3 PBD data are plotted for the polished surface. All parts of Fig. 3 show a regular behaviour from spot to spot. Thus, surface defects introduced by polishing are homogeneously distributed over the irradiated area. In Fig. 3a a correlation to SEM images is depicted: fracture covering the whole laser spot goes together with a strong increase of the deflection amplitude above  $10$   $\text{J}/\text{cm}^2$  indicating the development of a plasma. This corresponds well with light emission observable with the bare eye (Fig. 3b). In the fluence range between 5 and  $10$   $\text{J}/\text{cm}^2$  a slight linear increase of the deflection amplitude is detectable. The transit time in that range is constant showing a propagation of the signal with the speed of sound, caused by a photoacoustic wave (Fig. 3c). Just below the plasma

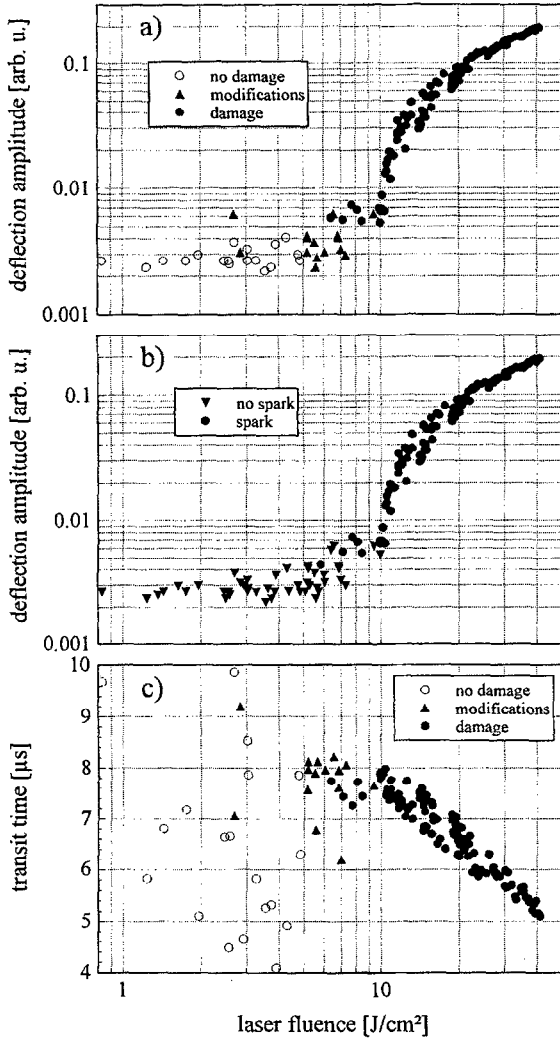


Fig. 3. Amplitudes (a), (b) and transit times (c) of the probe beam deflection for polished CaF<sub>2</sub>(111) irradiated with 248 nm/14 ns laser pulses. Each point represents a single shot. Classification of data spots is given according to SEM observations (a), (c) and the occurrence of visible light emission (spark) observed by eye (b).

onset, SEM microscopy exhibits starting of isolated cracks. This is in all cases connected with emission of light. But since the density of the emitted particles is too low a plasma cannot be ignited and only a small but definite photoacoustic signal is detected. Even at the lower end of the linear regime around 6 J/cm<sup>2</sup> a surface modification without topographical alterations shows up in the SEM (Fig. 4) in the form of charging. We emphasize that on uncoated surface such modifications are observable down to 3 J/cm<sup>2</sup>. Hence charging due to small differences in the secondary electron yield can sensitively reveal the very beginning of laser damage.

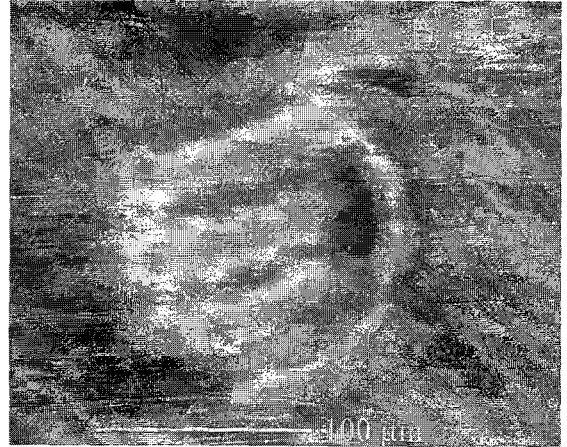


Fig. 4. SEM micrograph of CaF<sub>2</sub>(111) irradiated with a single laser pulse of 6.5 J/cm<sup>2</sup>. The uncoated surface sensitively reveals a change of the secondary electron yield although no topographical changes have taken place.

Another evidence for the high sensitivity of SEM in secondary electron mode is the observation of large cloudy areas outside the irradiated spots on uncoated insulator surfaces (Fig. 5a). Although there is a sharp contrast

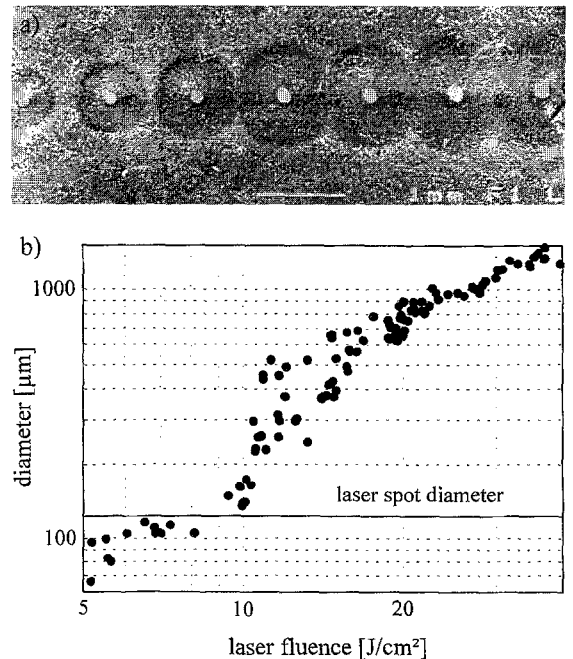


Fig. 5. SEM micrograph of uncoated, polished CaF<sub>2</sub>(111) displaying several spots, irradiated with fluences from 20 to 40 J/cm<sup>2</sup>, which show long-range surface modifications (a). The diameters of the courts are plotted in (b), showing a clear threshold at 10 J/cm<sup>2</sup> as in Fig. 3a.

resulting from a changed secondary electron yield, only a slight surface modification must have happened because detection was not possible with any other technique. Starting at the same fluence as the plasma onset the diameter of these charged regions increases dramatically and reaches 1 mm at the highest fluences (Fig. 5b). The good agreement of the plasma threshold in Fig. 3a and the beginning of this long-range surface modification suggests that these features are caused by shock waves. This proposal is corroborated by similar trends over the whole fluence range of the intensity dependence of the deflection amplitude (Fig. 3a) and the diameters of modified regions (Fig. 5b). A microscopic explanation for the change of secondary electron emission is still missing.

#### 4. Conclusions

The most prominent laser damage feature of polished and cleaved  $\text{CaF}_2(111)$  is cracking along the natural cleavage planes leading to mostly triangular shaped tiles. For cleaved samples a higher laser resistivity is observed. It can increase up to a factor of 4 but is affected by the density and height of steps. Polishing disturbs the crystalline structure in the near surface region leading to an enhanced absorption and a distinctly lower threshold for laser damage. This results in cracking which can be described by simple thermoelastic considerations. With photoacoustic deflection measurements and scanning electron microscopy of uncoated samples we were able to detect even minute damage features appearing below the threshold fluence for massive fracture, as well as surface modifications far outside the irradiated laser spot.

#### Acknowledgement

Part of this work was supported by the Deutsche Forschungsgemeinschaft, Sfb 337.

#### References

- [1] E. Matthias and R. Dreyfus, in: *Topics in Current Physics*, ed. P. Hess, vol. 47 (Springer Berlin, Heidelberg 1989) p. 89.
- [2] C.R. Giuliano, *Appl. Phys. Lett.* 5 (1964) 137.
- [3] R.C. Estler, E.C. Apel and N.S. Nogar, *J. Opt. Soc. Am. B* 4 (1987) 281.
- [4] B. Dietrich, E. Förster and R. Böttger, *Kristall und Technik* 12 (1977) 609 (in German).
- [5] H. Dunken and U. Kriltz, *Exp. Tech. Phys.* 39 (1991) 71 (in German).
- [6] O. Kreitschitz, W. Husinsky, G. Betz and N.H. Tolk, *Nucl. Instr. and Meth. B* 78 (1993) 327.
- [7] S. Gogoll, E. Stenzel, M. Reichling and E. Matthias, *AIP Conf. Proc.* 288 (1994) 50.
- [8] R.L. Webb, L.C. Jensen, S.C. Langford and J.T. Dickinson, *J. Appl. Phys.* 74 (1993) 2323.
- [9] R. Kelly, J.J. Cuomo, P.A. Leary, J.E. Rothenberg, B.E. Braren and C.F. Aliotta, *Nucl. Instr. and Meth. B* 9 (1985) 329.
- [10] M. Reichling, H. Johansen, S. Gogoll, E. Stenzel and E. Matthias, *Nucl. Instr. and Meth. B* 91 (1994) 628.
- [11] S. Gogoll, E. Stenzel, M. Reichling, H. Johansen and E. Matthias, *Appl. Surf. Sci.* 96–98 (1996) 332.
- [12] E. Matthias, J. Siegel, S. Petzoldt, M. Reichling, H. Skurk, O. Käding and E. Neske, *Thin Solid Films* 254 (1995) 139.
- [13] H. Johansen, S. Gogoll, E. Stenzel and M. Reichling, *Phys. Status Solidi A* 150 (1995) 613.
- [14] S.C. Jones, P. Braunlich, R.T. Casper and X.A. Shen, *Opt. Eng.* 28 (1989) 1039.
- [15] R.G. Bessent, W. Hayes, J.W. Hodby and P.H.S. Smith, *Proc. Roy. Soc. A* 309 (1969) 69.
- [16] M. Reichling and H. Grönbeck, *J. Appl. Phys.* 75 (1994) 1914.
- [17] A.A. Griffith, *Philos. Trans. Roy. Soc. A* 221 (1920) 163.
- [18] H.S. Bennett and C.D. Cantrell, *Appl. Opt.* 16 (1977) 2931.
- [19] R. Houwink, *Elastizität, Plastizität und Struktur der Materie* (Verlag Steinkopf, Dresden, Leipzig 1950) (in German).
- [20] D.J. Gallant, M. Law and B. Pond, NIST (U.S.), *Spec. Publ.* 752, Washington DC (1988) p. 159.
- [21] E. Eva and K. Mann, *Appl. Phys. A* 62 (1996) 143.